Journal of Hydrology: Regional Studies 64 (2026) 103214

Contents lists available at ScienceDirect

Journal of Hydrology: Regional Studies

journal homepage: www.elsevier.com/locate/ejrh

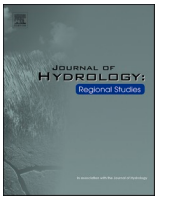

Meteoric water $\delta^{18}O$ across the Dinarides: Role of topography, air-mass mixing, and precipitation seasonality

Gabriela Sanchez Ortiz [a], Marlene Löberbauer [b], Nevena Andrić-Tomašević [c], Oleg Mandic [d], Davor Pavelić [e], Vedad Demir [f], Patrick W. Keys [g], Maud J. M. Meijers [b,*], Jeremy K.C. Rugenstein [a]

[a] Colorado State University, Department of Geosciences, Fort Collins, United States
[b] University of Graz, Department of Earth Sciences, NAWI Graz Geocenter, Graz, Austria
[c] Karlsruhe Institute of Technology, Institute of Applied Geosciences, Karlsruhe, Germany
[d] Natural History Museum Vienna, Geological-Paleontological Department, Vienna, Austria
[e] University of Zagreb, Faculty of Mining, Geology and Petroleum Engineering, Pierottijeva ul. 6, Zagreb 10000, Croatia
[f] Federal Institute for Geology - Sarajevo, Ilidža, Bosnia and Herzegovina
[g] Boston University, Department of Earth and Environment, Boston, United States

ARTICLE INFO

Keywords:
Dinarides
Water isotopes
Hydroclimate
Paleoaltimetry
Croatia
Bosnia and Herzegovina

ABSTRACT

Study region: Streams in the Dinarides ranging from coastal Croatia across the high-elevation basins of Bosnia and Herzegovina to the lee of the Dinarides.
Study focus: The topographic evolution of the Dinarides is poorly-constrained and its controlling geodynamic mechanisms remain unclear. The oxygen-isotope composition ($\delta^{18}O$) of authigenic minerals is a common paleo-altimeter for reconstructing past topography, proper interpretation requires thorough constraints on mechanisms modifying modern meteoric-water $\delta^{18}O$. To constrain modern $\delta^{18}O$ patterns across the Dinarides, we collected new stream samples and integrated them with published water stable isotope data.
New hydrological insights for the region: Meteoric-water data show $\delta^{18}O$ is higher at the coast (~-6 ‰) and lower at the peak (~-11 ‰). We use moisture trajectory models to show isotopic patterns across the Dinarides reflect two distinct moisture sources. The dominant source of moisture on the windward side originates from the Mediterranean and the leeward side has a continental source. This difference in moisture sources is reflected in d-excess values, which are high along the windward margin—reflective of Mediterranean moisture—and low in the lee, reflective of summertime, continental-sourced moisture. We interpret orographic rainout as the primary-driver of modern precipitation and surface water $\delta^{18}O$ with secondary influences from moisture sources and precipitation seasonality. Our findings have implications for understanding the climatic processes that deliver moisture as well as our understanding of the past topography of the Dinarides.

1. Introduction

The history of topography in tectonically active areas provides critical constraints on the geodynamic and climatic processes that

* Corresponding author.
E-mail address: maud.meijers@uni-graz.at (M.J.M. Meijers).

https://doi.org/10.1016/j.ejrh.2026.103214
Received 2 September 2025; Received in revised form 15 January 2026; Accepted 30 January 2026
Available online 4 February 2026
2214-5818/© 2026 The Authors. Published by Elsevier B.V. This is an open access article under the CC BY-NC-ND license (http://creativecommons.org/licenses/by-nc-nd/4.0/).

result in the formation of mountain ranges (Molnar and England, 1990; Willet, 1999). However, reconstructing the topographic history of mountain ranges remains difficult. Because mountains are continually subject to erosion, there remains no direct evidence of past orogen-scale topography. One commonly used method to reconstruct past topography is to rely upon the close association between topography and climate and use proxies that reflect past climate, thereby inferring changes in topography through their hypothesized impact on climate (Forest et al., 1995). For example, many ranges receive substantially more precipitation on their windward slopes than in their lee. Thus, any proxy of precipitation that tracks changes in windward or leeward precipitation may be used to infer topographic growth. The most common "paleo-altimeter" is the oxygen isotope composition ($\delta^{18}O$) of authigenic minerals. It relies upon this principle: Growing topography forces increasing orographic rainout, which preferentially removes ^{18}O from water-laden air-parcels. This rainout results in decreasing precipitation $\delta^{18}O$ values with elevation and lower leeside $\delta^{18}O$ values (Chamberlain and Poage, 2000; Rowley et al., 2001; Rowley and Garzione, 2007; Mix et al., 2011; Caves et al., 2015; San Jose et al., 2020).

However, there are a number of complications associated with using $\delta^{18}O$ paleoaltimetry as a tracer of past topography. Orographically induced drying of the atmosphere (*i.e.*, the formation of a rain shadow) can result in raindrops that experience post-condensation evaporation during hydrometeor fall or in evaporative soil waters, thereby increasing $\delta^{18}O$ values even as topography rises (Blisniuk and Stern, 2005; Lee et al., 2012; Kelson et al., 2023). Topographic growth often modifies precipitation seasonality due to changed interactions between atmospheric moisture transport and orography (Baldwin and Vecchi, 2016; Schiemann et al., 2009). In the mid-latitudes, this can translate into different seasonal $\delta^{18}O$ values being recorded by proxies depending upon when those proxies form (Caves et al., 2017; Kukla et al., 2022; Rugenstein et al., 2022; Driscoll et al., 2024), thereby decoupling topographic growth from decreasing $\delta^{18}O$ values in meteoric waters. Topographic growth can additionally rearrange atmospheric circulation, resulting in changes in air mass mixing and further decoupling $\delta^{18}O$ from topographic growth (Lechler and Galewsky, 2013; Mix et al., 2019). Regional and global climate change may also change precipitation seasonality as well as modify atmospheric circulation.

One method to constrain the complications associated with using $\delta^{18}O$ paleoaltimetry is to understand the mechanisms that today generate changes in precipitation and surface water $\delta^{18}O$ values across modern mountain ranges. In this contribution, we focus on the Dinarides (Fig. 1), a range which stretches from the southern Alps in Slovenia to the Hellenides in northern Greece, with elevations up to 2500 m. The Dinarides are a mountain belt formed as part of the Alpine-Himalayan chain during subduction associated with the closure of the Tethys Sea (Bennett et al., 2018; Šumanovac et al., 2017; Handy et al., 2019). Shortening events during the Cretaceous up to the Eocene resulted in thickening of the continental crust (Pamić, 2002; Schmid et al., 2008; Andrić et al., 2017). During the Early

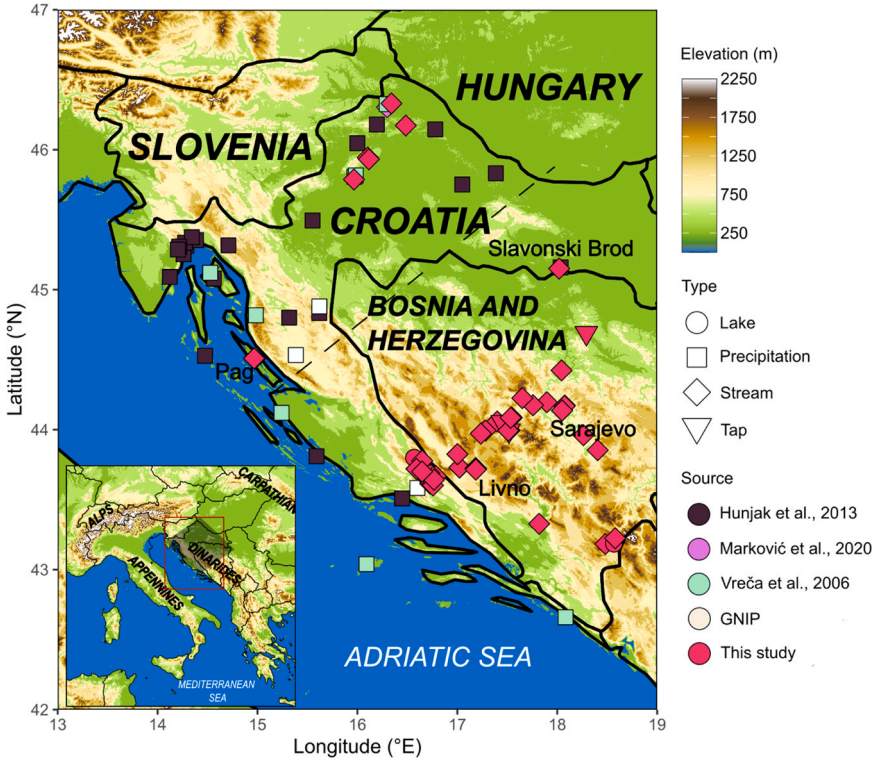

Fig. 1. Study area in the Dinaric Alps. Diamonds show the 59 stream water samples we collected in the summers of 2022 and 2025. Water types are denoted by different symbols; fill colors denote different studies (published and new). Samples from Marković et al., (2020) are concentrated in northern Croatia and plotted below our study points. Dashed line shows the boundary between northern (points northwest of the dashed line) and southern samples (points southeast of the dashed line). Inset map shows the location of the study area (red square) in relation to mountains in central and southern Europe. Black transparent square shows the area over which the swath profile was calculated (see Fig. 4C, D).

Miocene, a series of intramontane basins formed, filled with lakes, as a result of extension in the Pannonian Basin north of the Dinarides (Mandic et al., 2009; de Leeuw et al., 2012). These freshwater lacustrine basins formed along the Dinaridic western margin—collectively called the Dinaric Lake System (DLS)—and hosted a highly biodiverse endemic fauna (de Leeuw et al., 2011; Harzhauser et al., 2012; Mandic et al., 2009, 2020). The eastern margin of the Dinarides hosted saline lakes—called the Serbian Lake System (SLS, Krstić et al., 2012; Harzhauser and Mandic et al., 2008; Neubauer et al., 2020). However, the topographic evolution of the Dinarides, as well as the climate that sustained freshwater lakes on the windward side and saline lakes on the leeward side during the Miocene remain poorly constrained.

Many of these basins host thick successions of lacustrine carbonates. Carbonates formed in the presence of meteoric waters record the isotopic composition of the waters that formed them. Towards the goal of constraining the history of surface topography in the Dinarides, we present 59 new stable hydrogen (δ^2H) and oxygen ($\delta^{18}O$) isotopic data from surface water samples that span the Dinarides, from the Adriatic Sea to Sarajevo (Croatia to Bosnia and Herzegovina), to understand the modern-day pattern of δ^2H and $\delta^{18}O$ in precipitation across the range. These new data fill a critical spatial gap in our knowledge of meteoric water stable isotopes across the Dinarides. In particular, our new data targets streams in the highest portion of the Dinarides and from Bosnia and Herzegovina. There has been little stable isotope hydrology research in these areas and also notably little stream water isotope data published in SE Europe. We combine our new data with previously published precipitation and surface water $\delta^{18}O$ and δ^2H data (n = 734) and with new modeling of moisture sources, using a Water Accounting Model-2layers (WAM) (van der Ent et al., 2010; van der Ent and Savenije, 2013) and trajectories, using a Hybrid Single-Particle Lagrangian Trajectory (HYSPLIT) model (Draxler and Hess, 1998), to constrain the mechanisms that generate changes in isotopic values from the Adriatic coast to the southeastern European interior. This modeling is the first attempt to combine analysis of HYSPLIT and WAM to generate a coherent source-to-trajectory interpretation of water isotopes. We find that waters with higher δ^2H and $\delta^{18}O$ values are closest to the coast, whereas lower δ^2H and $\delta^{18}O$ values are found at the crest of the range and in the lee of the range. We attribute this spatial pattern dominantly to orographic-forcing of moisture-bearing air parcels that originate in the Mediterranean Sea, though air mass mixing with continental moisture modifies leeward isotopic compositions of surface waters and precipitation. We conclude that orographic effects today control precipitation and surface water δ^2H and $\delta^{18}O$ in the Dinarides.

2. Background

2.1. Climatic setting

Today, the shape and altitude of the Dinarides in relation to the Adriatic and Mediterranean controls much of the climate in the

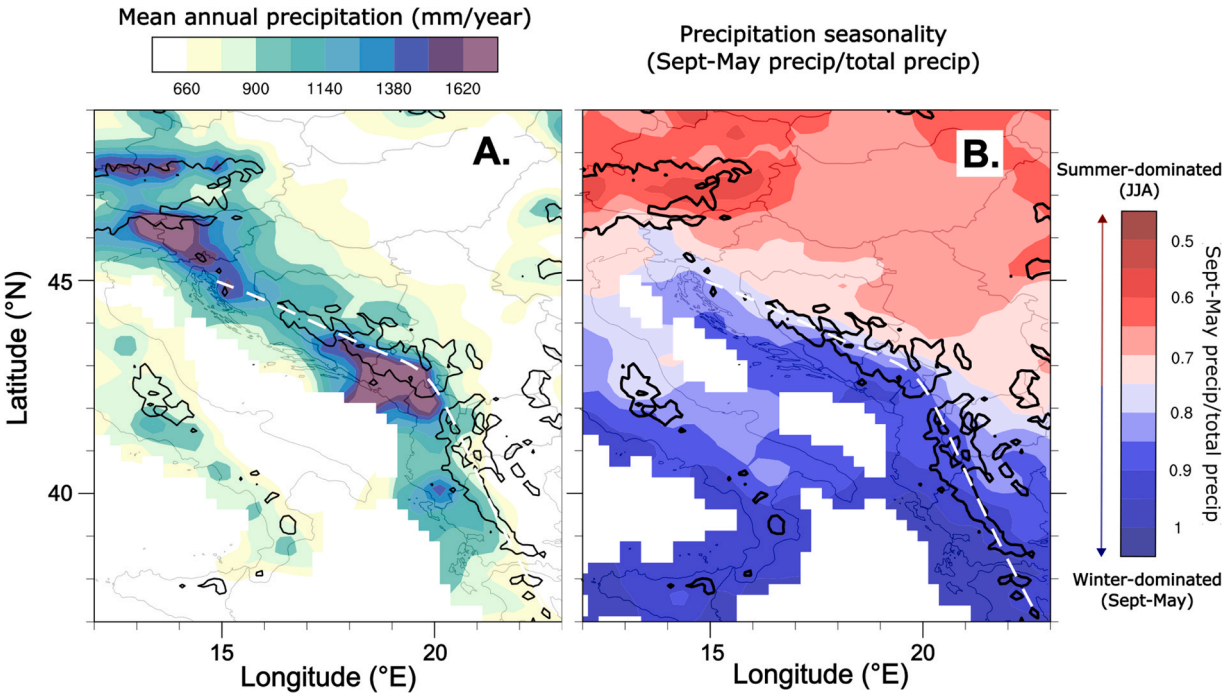

Fig. 2. A) Mean annual precipitation (mm/year) across the Dinarides. B) Seasonality of the precipitation (fraction of precipitation that falls between September and May over the total precipitation. Red colors represent summer-dominated (JJA) moisture. Black line is the smoothed 1000 m contour line. Country borders shown in thin gray outline. White dashed line indicates the approximate boundary between the windward and leeward sides of the Dinarides.

region (Zaninović et al., 2008). The windward side of the Dinarides is one of the wettest regions in Europe with parts of the Dinarides receiving greater than 3000 mm of precipitation annually (Fig. 2). Nearly all of this windward precipitation falls during the cool season (i.e. between Sept. and May). In contrast, the leeward side of the Dinarides is substantially drier and receives nearly half of its precipitation in the warm season (i.e., June, July, and August; Fig. 2B). In the high-elevation basins of the Dinarides, much of the

Table 1
Stream water samples collected from the Dinarides in the summer of 2022 and 2025.

Sample	Latitude	Longitude	Distance from coast (km)	Mean elevation[a] (m)	Max elevation[a] (m)	$\delta^{18}O$ (‰, VSMOW)	$\delta^{2}H$ (‰, VSMOW)	Type	Collection date
PGW1	44.507	14.972	0	32	180	-5.4	-31.2	Stream	7/3/22
PGW2	44.507	14.972	0	32	180	-5.6	-31.1	Stream	7/3/22
PGW3	44.508	14.968	0	33	162	-5.8	-34.2	Stream	7/3/22
PGW4	44.508	14.968	0	33	162	-5.8	-32.3	Stream	7/3/22
PGW5	44.509	14.967	0	33	162	-5.7	-32.8	Stream	7/3/22
PGW6	44.509	14.967	0	33	162	-5.5	-30.9	Stream	7/3/22
PGW7	44.509	14.967	0	33	162	-6	-33.9	Stream	7/3/22
SW1	43.72	16.591	23	639	932	-6.3	-38.3	Stream	7/4/22
SW2	43.704	16.64	27	379	486	-8.3	-51.3	Tap	7/4/22
BW3	43.994	17.517	84	694	902	-10.5	-67.2	Tap	7/5/22
BW4	43.993	17.51	84	1210	2095	-10.1	-66.4	Stream	7/5/22
BW5	44.058	17.399	89	1114	1749	-9.6	-61.8	Stream	7/5/22
BW6	43.994	17.282	78	1358	1647	-10	-63.5	Stream	7/5/22
BW7	43.972	17.235	75	1237	1647	-9.5	-61.1	Stream	7/5/22
BW8	44.054	17.449	87	963	1749	-10.6	-69.4	Tap	7/6/22
BW9	44.086	17.545	93	1140	1480	-10.9	-72.2	Stream	7/7/22
MW1	43.73	17.022	41	866	906	-8	-47.7	Stream	7/6/22
MW2	43.73	17.022	41	866	906	-8	-48	Stream	7/6/22
LW3	43.825	17	51	1113	1372	-9.1	-57	Stream	7/5/22
OZW1	43.725	17.183	44	1236	1612	-7.4	-45.7	Stream	7/7/22
OZW2	43.719	17.186	44	971	1003	-8.5	-51.8	Stream	7/7/22
OZW3	43.719	17.185	44	1223	1612	-8.4	-51.1	Stream	7/7/22
OZW4	43.715	17.184	43	1214	1612	-8	-48.5	Stream	7/7/22
KAW1	44.171	18.072	131	859	1291	-9.6	-64.1	Stream	7/8/22
KAW2	44.171	18.072	132	758	971	-9.1	-59.1	Stream	7/8/22
KAW3	44.169	18.073	130	697	956	-8.9	-58.4	Stream	7/8/22
KAW5	44.137	18.048	124	930	2083	-10.8	-73.1	Stream	7/9/22
KAW6	44.137	18.048	124	930	2083	-10.5	-71.4	Stream	7/9/22
ZW1–25	45.787	15.965	164	116	131	-8.5	-55.78	Stream	8/10/25
SW1–25	43.720	16.591	50	707	955	-5.9	-35.14	Stream	8/15/25
SW3–25	43.668	16.785	53	873	1483	-5.9	-38.26	Stream	8/11/25
SW4–25	43.689	16.719	52	1053	1836	-6.6	-41.38	Stream	8/11/25
SW5–25	43.799	16.566	59	426	488	-6.9	-45.24	Lake	8/12/25
SW6–25	43.615	16.728	44	739	1895	-7.5	-47.34	Stream	8/12/25
SW7–25	43.602	16.756	43	438	641	-5.4	-36.29	Stream	8/12/25
SW8–25	43.697	16.641	49	496	825	-2.9	-23.06	Stream	8/12/25
SW9–25	43.700	16.647	51	377	487	-6.3	-40.31	Tap	8/12/25
SW10–25	43.643	16.766	49	695	1465	-6.6	-40.92	Stream	8/13/25
SW11–25	43.778	16.648	59	1017	1448	-7.8	-48	Stream	8/15/25
SW12–25	43.700	16.647	51	377	487	-6.5	-40.11	Stream	8/16/25
LW1–25	43.825	17.000	78	880	1148	-8.9	-55.36	Stream	8/16/25
MSW1–25	43.328	17.818	80	1053	2200	-8.4	-52.21	Stream	8/16/25
GOW1–25	43.183	18.481	83	930	988	-3.3	-21.81	Stream	8/16/25
GOW2–25	43.186	18.567	83	1136	1224	-6.7	-42.25	Lake	8/17/25
GOW3–25	43.224	18.579	94	1369	1715	-8.5	-51.61	Stream	8/17/25
SJOW1–25	43.853	18.404	161	677	908	-9.3	-61.67	Stream	8/17/25
IW1–25	43.960	18.262	175	1014	2074	-9.2	-61.59	Stream	8/17/25
ZNW1–25	44.196	17.895	155	703	1328	-8.5	-57.23	Stream	8/18/25
BLW1–25	44.174	17.757	148	1110	1932	-9.4	-62.94	Stream	8/18/25
TW1–25	44.225	17.650	146	973	1850	-9.5	-64.07	Stream	8/18/25
BW4–25	43.993	17.510	118	1211	2099	-9.9	-64.95	Stream	8/18/25
BW10–25	44.085	17.533	129	1138	1511	-10.8	-72.44	Stream	8/18/25
ZPW1–25	44.424	18.043	185	889	2090	-9.0	-60.36	Stream	8/18/25
GAW1–25	44.691	18.291	220	368	692	-10.1	-69.71	Tap	8/18/25
SBW1–25	45.151	18.019	259	447	2099	-8.6	-56.93	Stream	8/19/25
VW1–25	46.331	16.340	212	179	198	-10.4	-71.93	Stream	8/19/25
KLW1–25	46.173	16.484	211	359	446	-9.7	-64.16	Stream	8/20/25
MVW1–25	45.944	16.102	171	391	591	-8.6	-56.88	Stream	8/22/25
MVW2–25	45.932	16.114	170	406	723	-9.6	-63.9	Stream	8/22/25

[a] The mean and max elevations are calculated using the corresponding hypsometry of the upstream drainage basin.

wintertime precipitation arrives as snow, and for much of the winter, mean snow depths are greater than 1 m. Mean monthly temperatures are also partly modified by the presence of the Dinarides. Along the coast and on the windward flanks of the Dinarides, mean monthly temperatures vary by less than 10°C over the course of the year, whereas regions leeward of the Dinarides are more continental and experience > 20°C changes in mean monthly temperatures between summer and winter (Zaninović et al., 2008).

2.2. Geologic setting

The Dinarides are an orogenic fold-and-thrust belt formed as part of the Alpine-Himalayan chain following the closure of one branch of the Tethys Sea due to the collision between the Adriatic and Eurasian plates (Bennett et al., 2018; Šumanovac et al., 2017; Handy et al., 2019). Shortening lasted from the Cretaceous up to the Oligocene (Pamić, 2002; Schmid et al., 2008, Andrić et al., 2017). During the Early Miocene, a series of intramontane basins formed freshwater lakes occupying depressions across the Dinarides (Mandic et al., 2009; de Leeuw et al., 2012). Based on the highly diverse endemic fauna, these lacustrine basins are divided into two systems: the Dinaric Lake System (DLS) and the Serbian Lake System (SLS), mainly occupying the external and internal part of the Dinarides, respectively (Krstić et al., 2003, 2012; de Leeuw et al., 2011; Harzhauser et al., 2012; Mandic et al., 2009, 2020). Current sedimentological (Obradović et al., 1997; Pavelić et al., 2016, 2022; Andrić-Tomašević et al., 2021) and paleontological (Krstić et al., 2003; Neubauer et al., 2015a, 2015b, 2015c, 2020) observations suggest that these basins developed under contrasting environmental conditions in the internal and external Dinarides, also corresponding roughly to their present day windward and leeward sides (Burić, 2010). In this context, Andrić-Tomašević et al. (2021) proposed that during the evolution of the lacustrine systems, the Dinarides were high enough to act as an orographic barrier preventing the moisture from the Adriatic Sea from reaching the internal part of the range.

3. Methods

3.1. Stream water sampling and analysis

We collected 28 water samples from streams and springs ranging across the Dinarides from the Adriatic coast to Sarajevo (Table 1) in early July 2022 and another 31 samples in middle August 2025. Sampling locations varied in elevation from sea level up to 1000 m. As a check on any temporal variations in our sites, we recollected samples in 2025 from three sites (SW1, LW1, and BW4) that we had visited in 2022. Collection from lakes and reservoirs was avoided since evaporation has been shown to have a strong effect on the isotopic composition of lake waters due to their longer residence times (Leng and Marshall, 2004). We delineated the watershed where the sample is located, calculated the max and mean hypsometric elevations of points upstream of the sampling location using built-in functions in Topographic Analysis Kit and TopoToolbox (Schwanghart and Scherler, 2014; Forte and Whipple, 2019).

All samples were filtered through 0.22 μm filters, stored in 2 mL vials, wrapped with Parafilm, and refrigerated before analysis. We measured $\delta^{18}O$ and $\delta^{2}H$ using a Picarro L-2130i Water Isotope Analyzer coupled to a High Precision Vaporizer housed at the CSU Natural Resource Ecology Lab EcoCore Facility. Approximately 1.8 μL aliquots of sample were injected seven times; results are the average $\delta^{18}O$ and $\delta^{2}H$ for the last four injections. Values of $\delta^{18}O$ and $\delta^{2}H$ were corrected based upon measurements of USGS standards 45, 46, and 47. The analytical precision is better than 0.2 ‰ (2σ) for $\delta^{18}O$ and 0.5 ‰ (2σ) for $\delta^{2}H$.

3.2. Compilation of published $\delta^{18}O$ and $\delta^{2}H$ data and analysis

We combine our data with published groundwater, lake, precipitation, and river/stream samples (Table S1; Vreča et al., 2006; Hunjak et al., 2013; Marković et al., 2020). We also use data from the Global Network of Isotopes in Precipitation (GNIP), accessible from the Croatian Geological Survey and the International Atomic Energy Agency (IAEA). To account for the resulting disparity in data density between northern Croatia and southern Croatia/Bosnia and Herzegovina (Fig. 1) and to test for latitudinal differences in the data trends, we first analyze the data by splitting all of the data into two separate transects. These transects are separated by the dashed line shown in Fig. 1.

3.3. HYSPLIT simulations

Because the isotopic composition of precipitation is influenced by moisture source and pathway, we used the National Oceanic and Atmospheric Administration's (NOAA) HYSPLIT model (Draxler and Hess, 1998) to track the trajectory of air parcels backward from a given location. We used climate data from the Global Data Assimilation System (GDAS), which offers the highest-resolution (1° x 1°), multi-year global climate dataset available for HYSPLIT simulations. We simulate back-trajectories from two locations in Croatia and Bosnia: (1) Pag in Croatia and (2) Sarajevo in Bosnia and Herzegovina (Fig. 3; Figure S1). Both sites were chosen for being representative of the windward (Pag) and leeward (Sarajevo) sides of the Dinarides. We initialize air parcels at 1000 m above ground level and run the simulation backwards for 7 days. A back-trajectory is simulated every 6 h for the time period from 2005 to 2016. We filter our results for only those trajectories that are estimated to have produced precipitation within 6 h of arriving at the site. Results are presented as 2D-density-contours of precipitation-producing air parcels, binned by 0.5° x 0.5°. HYSPLIT has been used extensively to understand the sources and pathways of moisture and the consequent effects on precipitation and meteoric water $\delta^{18}O$ (Sjostrom and Welker, 2009; Oster et al., 2012; Lechler and Galewsky, 2013; Caves et al., 2017; Driscoll et al., 2024). Nevertheless, we note that HYSPLIT does not track moisture, but rather all air masses, including those with a low specific humidity (Stein et al., 2015). This means that sources of moisture can only be inferred from HYSPLIT, since HYSPLIT does not track where the moisture is taken up by air parcels

via evapotranspiration or any upwind loss by precipitation or diffusion of moisture into surrounding air parcels.

3.4. WAM modeling

To supplement our HYSPLIT simulations with a model that does track moisture, we used the WAM (van der Ent et al., 2010; van der Ent and Savenije, 2013) to estimate the source of moisture in the Dinarides. The WAM uses high resolution (0.25° x 0.25°) data from the ERA5 climate reanalysis to backtrack the origin of precipitation in a specific sink region (Dee et al., 2011; Keys et al., 2012). The WAM uses hourly data for horizontal and vertical wind, humidity, surface pressure, total column water evaporation, and total precipitation (Keys and Wang-Erlandsson, 2018; Keys et al., 2018). For each grid cell and its corresponding air column, the amount of evaporation entering a grid cell is accounted for, then the evaporated water mixes within the column, and exits as precipitation or as moisture transported to another grid cell. As such, the WAM indicates the amount of moisture recycling in a region. We ran the WAM on two zones (outlined in white in Fig. 3) that extend along the windward (Pag) or leeward (Sarajevo) sides. The amount of water that evaporated in every pixel and then rained out in the area of interest is shown as shading in Fig. 3.

4. Results

4.1. HYSPLIT and WAM precipitation trajectories

At our back-trajectory sites, there are multiple trajectories where air parcels originate in the Mediterranean Sea and also multiple trajectories that originate to the north and east over the European continent. Of the Mediterranean trajectories, one passes over Italy and the Apennines before reaching our sites, whereas the other trajectory traverses the length of the Adriatic Sea (Fig. 3A). Trajectories showed minimal variability seasonally at each site (Figure S2). Though the two sites appear similar, Pag, which sits on the Adriatic coast, receives fewer trajectories from continental Europe, particularly in comparison with Sarajevo, which sits leeward of the Dinarides. However, even the leeward sites receive a substantial fraction of their moisture from trajectories that originate in the Mediterranean and traverse the Dinarides. Results of the moisture backtracking from the WAM correlate with the air parcel trajectories of the HYSPLIT model. The precipitation that falls on the windward side of the Dinarides is dominantly sourced from the Mediterranean evaporation. In contrast, the leeward side of the Dinarides receives less moisture than the windward side (Fig. 2A), but the precipitation that does fall on the leeward side is sourced mostly locally from terrestrial evapotranspiration; however, there is still a large portion of the annual precipitation that originates from evaporation in the Mediterranean (Fig. 3B).

We note that both HSYPLIT and WAM are models with a number of uncertain parameters. We intentionally chose a large sink area that encompasses much of the leeward and windward sides of the Dinarides in our WAM modeling to overcome any grid-scale resolution issues. To test the sensitivity of our HYSPLIT results, we performed several tests, including modifying the location of the

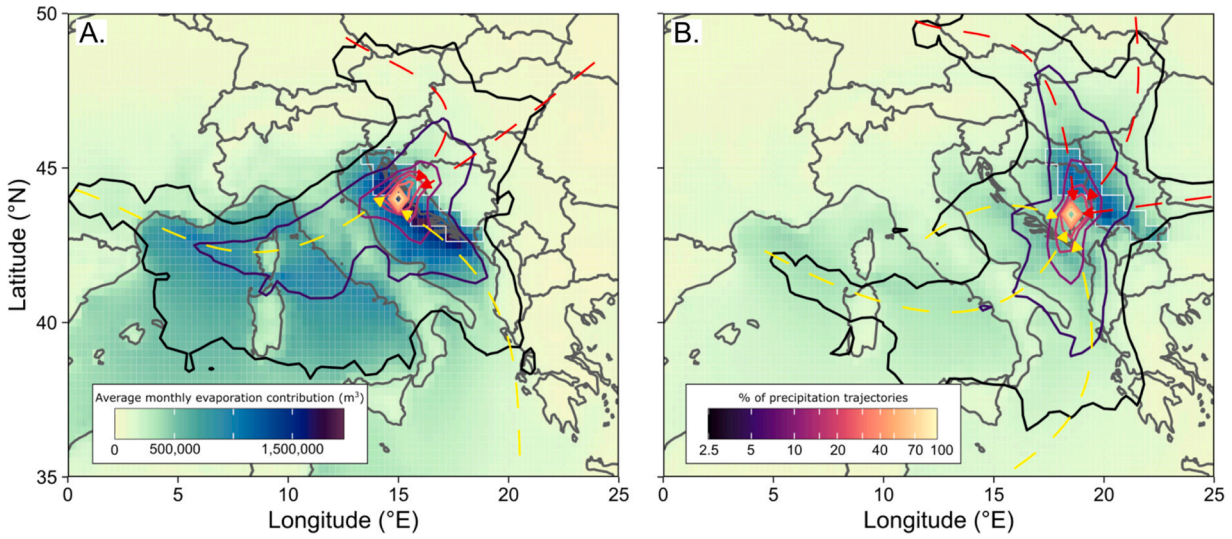

Fig. 3. HYSPLIT and WAM model results. HYSPLIT results are shown with colored contours and colored, dashed arrows; background shading shows the WAM results. HYSPLIT results include only trajectories for precipitation-producing air parcels. Back-trajectories were simulated from the windward (**A**; Pag, Croatia; n = 4931) and leeward (**B**; Sarajevo, Bosnia and Herzegovnia; n = 6131) side of the Dinarides. Arrows represent the most common observed trajectories. Yellow arrows represent trajectories originating from the Mediterranean Sea. Red arrows are continental trajectories. Colored density contours show the fraction of precipitation trajectories. Precipitation-producing trajectories are binned by 0.5° x 0.5° to produce density contours. Background shading is the evaporative contribution to precipitation on either the windward (**A**) or leeward (**B**) side of the Dinarides as simulated by WAM. Precipitation sink region is shown in thin white outline and represents the area over which the evaporative contribution is calculated. See also Figure S1 for only the HYSPLIT results for these sites.

endpoints (Figure S4) and changing the number of prior hours used when filtering trajectories for precipitation (Figure S3). As can be seen in these figures, our results are not sensitive to these parameters and suggest that HYSPLIT is robustly recording dominantly Mediterranean moisture sources on the windward slopes of the Dinarides and a mixture of Mediterranean and continental moisture sources on the leeward side of the Dinarides.

4.2. Stable isotopes ($\delta^{18}O$ and $\delta^{2}H$) and d-excess

Along both the northern and southern transects (see dashed line in Fig. 1), surface water $\delta^{18}O$ values decrease with distance from the coast, with the highest values (~ −6 ‰) at the Adriatic coast and the lowest values (~ −11 ‰) in surface waters collected near the modern crest of the range (100 km away from the coast) (Fig. 4A, B). Further from the coast, surface waters have lower $\delta^{18}O$ values (~ −9 ‰) than those at the coast, but higher than at the crest of the range (Fig. 4A, B). Between the coast and the highest elevation portion of the Dinarides (*i.e.*, the windward side) there is a gradient of approximately −2.97 ‰/km of elevation (intercept = −5.83 ‰, R^2 = 0.6565) when using the mean basin elevation and approximately −2.30 ‰/km of elevation (intercept = −5.67 ‰, R^2 = 0.672) when using the maximum basin elevation. Examining only the published precipitation data indicates a similar trend, with precipitation $\delta^{18}O$ decreasing by −2.60 ‰/km in windward stations and −3.90 ‰/km in leeward stations (Hunjak et al., 2013). Leeward of the crest of the Dinarides, precipitation $\delta^{18}O$ increases slightly and plateaus at a value of approximately −9 ‰ (Fig. 4).

Deuterium-excess (d-excess) is a second-order parameter often used to estimate the origin of waters or degree of evaporation and is defined as d-excess = $\delta^{2}H - 8*\delta^{18}O$ (Dansgaard, 1964). The highest d-excess values are found near the crest of the Dinarides and range from 12 ‰ to 16 ‰ (Fig. 5A, Figure S5). Coastal samples—which were collected at low elevations—have d-excess values of around 11 ‰. The lowest d-excess values are those from low elevation areas in the lee of the range such as the northern Croatian plains. The spatial trend is d-excess values generally increase with elevation (Fig. 5B). Stream water samples tend to have greater d-excess values compared to the precipitation samples collected at similar elevations. The general spatial pattern of d-excess is that low d-excess values are found in low-elevation areas in the leeward side of the Dinarides, while higher d-excess values are found in both high-elevation areas and the coast (Fig. 6B).

5. Discussion

5.1. Local Meteoric Water Line

The relationship between $\delta^{2}H$ and $\delta^{18}O$ of meteoric waters is globally defined by the Global Meteoric Water Line (GMWL) (Dansgaard, 1964), which is represented as $\delta^{2}H = 8*\delta^{18}O + 10.0$. Samples that define a line with a slope substantially less than 8 are thought to be impacted by kinetic fractionation processes, such as evaporation (Sharp, 2017; Putman et al., 2019). The data from the

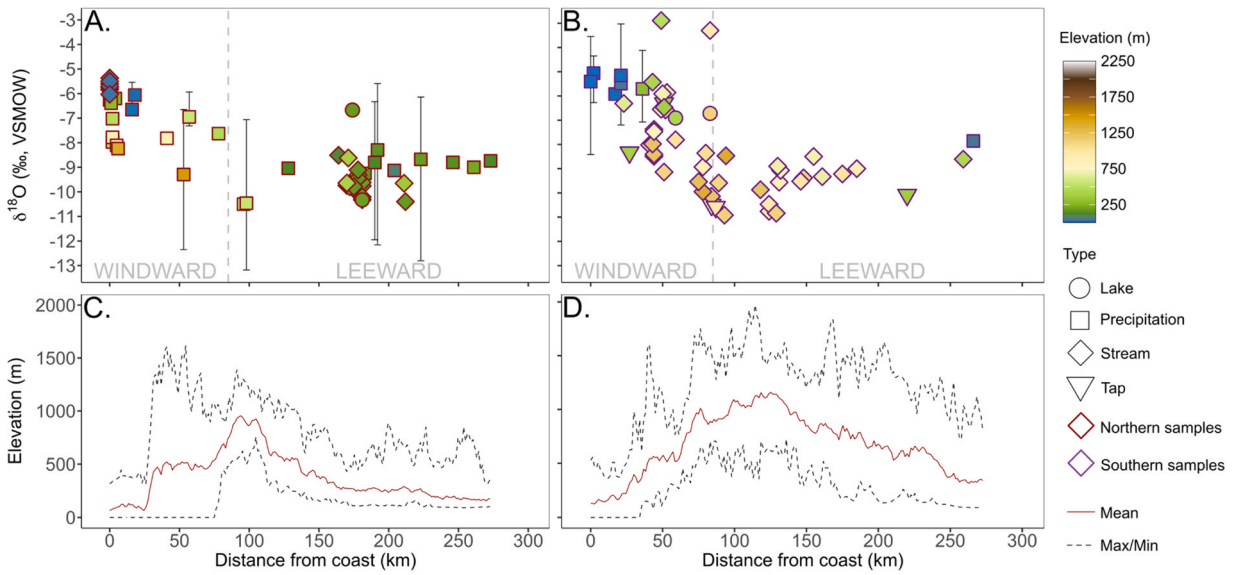

Fig. 4. Modern $\delta^{18}O$ gradient and elevation (m) of the northern (**A**) and southern (**B**) Dinarides plotted against distance from coast (km). $\delta^{18}O$ decreases inland. Higher $\delta^{18}O$ values are observed at the coast, while lower $\delta^{18}O$ values are seen at the crest of the range. Points represent values of samples obtained from the various types of water including lakes (circles), precipitation (squares), streams (diamonds), and tap water (inverted triangles). Error bars on the precipitation data (from Vreča et al. 2006) represent the unweighted mean winter (low) and summer (high) values. Points are colored by mean basin elevation (m). Points highlighted in red were collected in the summers of 2022 and 2025. Elevation profile of modern Dinarides topography across a 250 km north (**C**) and south (**D**) transect. Dashed lines in C and D are the minimum and maximum elevation along the swath profile; thin red line is the mean elevation along the swath profile.

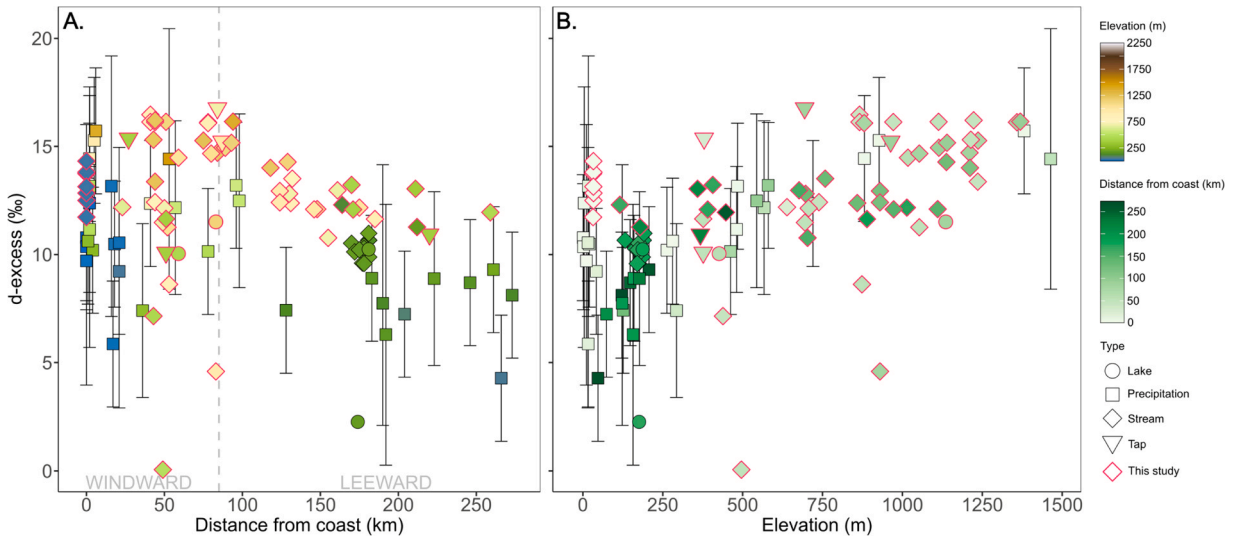

Fig. 5. A) Deuterium-excess (d-excess, ‰) plotted against distance from coast (km). Higher d-excess is seen at the crest of the range and lower d-excess in lowland areas in the lee of the Dinarides. **B)** d-excess plotted against mean basin elevation (m). In both panels, points represent unweighted mean values of precipitation samples and shape refers to the type of water sample. Error bars are 1σ for the precipitation data.

northern portion of our study area—where basins are close to the coast and have lower elevations—plot on a local meteoric water line (LMWL) with a slope of 8.4 and an intercept of 13.9 ‰ (Fig. 7). In contrast, data from the southern portion of our study area—where the higher elevation basins are located—plot on a LMWL with a slope of 7.0 and an intercept of 4.5 ‰ (Fig. 7). We note that two of our samples collected in 2025 fall well off the meteoric water line, with high $\delta^{18}O$ and $\delta^{2}H$. Though both of these samples are stream waters, their low d-excess indicates that these streams source water from an evaporative body upstream of our sampling site.

The close resemblance of these LMWLs to the GMWL suggests that neither the samples from the northern nor the southern transect have been substantially affected by evaporation (Putman et al., 2019). The lower slope of the southern transect LMWL (~ 7) appears to be caused by co-variation in d-excess, elevation, and $\delta^{18}O$. In short, higher elevation samples have low $\delta^{18}O$ and higher d-excess (Fig. 5B), resulting in these samples plotting well above the GMWL and causing a consequently lower slope. This analysis further

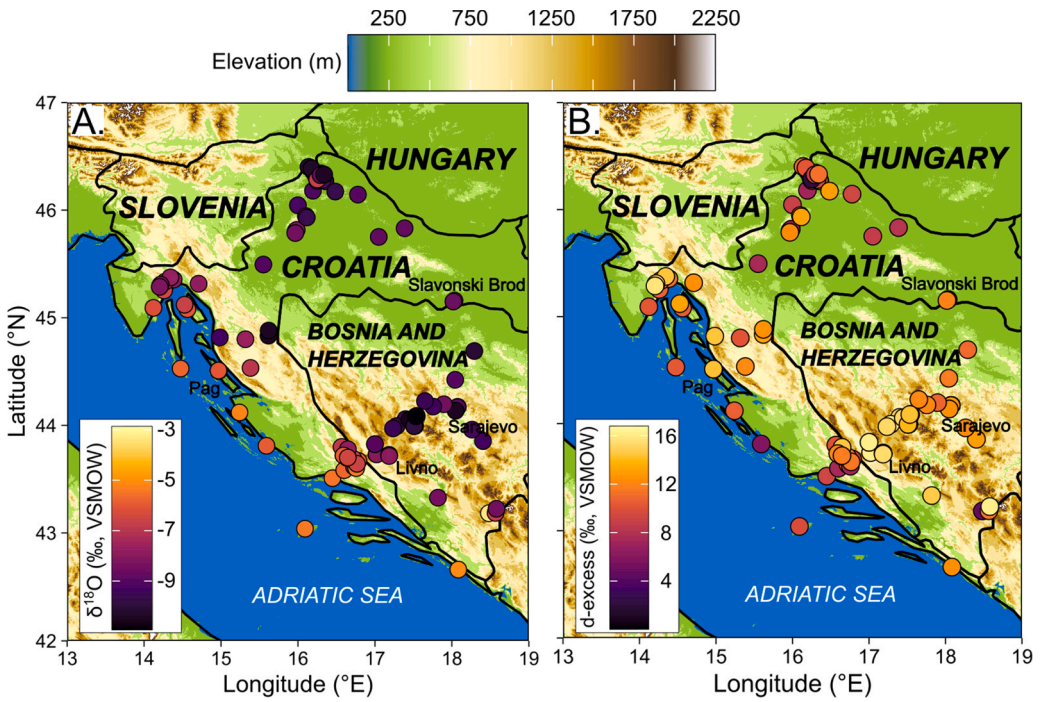

Fig. 6. Spatial distribution of $\delta^{18}O$ (**A**) and d-excess (**B**) in meteoric waters.

indicates that stream and spring waters adequately capture the precipitation $\delta^{18}O$ signal across the Dinarides. Indeed, stream water samples have $\delta^{18}O$ values that overlap with the mean precipitation $\delta^{18}O$ values along the entire transect across the Dinarides (Fig. 4). A direct comparison between stream water and precipitation isotope values is somewhat obscured by the fact that our new stream water isotope data cover a much higher elevation range (and are generally located further south) than existing precipitation isotope data (Figure S6). Nevertheless, similar trends are apparent in isotope data from both types of waters. Such close agreement between stream/river water samples and precipitation $\delta^{18}O$ likely occurs due to the high mean annual precipitation in the region relative to rates of potential evapotranspiration (Zaninović et al., 2008) as well as the generally karstic environment (particularly on the windward side of the Dinarides), which ensures high throughflow of water with limited potential for evaporation. The karstic environment of the region could allow for the possibility that stream water may originate from different watersheds across the basins. However, given the scale of our analysis (i.e., across the entire orogen), we anticipate that this cross-watershed mixing does not impact our conclusions. Research in other orogens has similarly found that stream water $\delta^{18}O$ and $\delta^{2}H$ are approximate recorders of mean annual catchment precipitation $\delta^{18}O$ and $\delta^{2}H$ (Hoke et al., 2014; Zhu et al., 2018; Spaur et al., 2025). Intriguingly, our new stream water d-excess data is marginally higher than nearby mean annual precipitation d-excess (though well within the annual range of observed precipitation d-excess values) (Fig. 5). This supports the notion that streams are recharged dominantly by wintertime moisture, which has a higher d-excess (see Section 5.2).

5.2. *Sources of moisture across the Dinarides*

Our new water $\delta^{18}O$ and $\delta^{2}H$ data—combined with our HYSPLIT and WAM modeling—suggest that there are two primary sources of moisture to the Dinarides: a dominant one from the Mediterranean on the windward side and a more continental source on the leeward side. These sources are reflected in the trend of meteoric water $\delta^{18}O$ values from the Adriatic coast to the leeside of the range. The steady decrease in meteoric water $\delta^{18}O$ values between the Adriatic coast and the crest of the Dinarides reflects rainout as moisture-laden air parcels lose moisture due to orographic forcing. To the east of the crest of the Dinarides, meteoric water $\delta^{18}O$ values increase slightly (~ 2 ‰), but remain lower than $\delta^{18}O$ values at the Adriatic coast. This suggests that leeside meteoric waters are a mixture of moisture that has traversed the high Dinarides from the Mediterranean Sea and continental European moisture sources which deliver higher $\delta^{18}O$ precipitation.

The predominance of Mediterranean-derived moisture throughout the region is supported by the $\delta^{2}H$ and d-excess data. Most of the data within 100 km of the coast has relatively high d-excess values (Fig. 6B); such high d-excess values are thought to originate from evaporation sourced from the Mediterranean, which enriches the lower atmosphere in ^{2}H (Gat and Carmi, 1970; Gat and Dansgaard, 1972; Gat et al., 2003; Liotta et al., 2006; Gat, 2010; Pfahl and Sodemann, 2014; Masiol et al., 2021; Natali et al., 2022). This vapor then feeds wintertime storms which supply most of the precipitation on the windward side of the Dinarides. Beyond approximately 100 km, d-excess values decline, and lower d-excess values are particularly prominent in the low-elevation plains of northern Croatia (Fig. 6B). This difference in d-excess values between the windward and leeward sides of the Dinarides likely reflect a combination of different moisture sources and different precipitation seasonalities. Indeed, our HYSPLIT and WAM results suggest that sites leeward of the Dinarides receive more moisture from continental Europe than do sites on the windward side of the Dinarides. These continental Europe trajectories are less affected by orographic rainout since they come through the low passes of the Alps-Carpathian range north of the Dinarides (Fig. 3B; see inset map of Fig. 1). Further, the Dinarides define a stark precipitation seasonality boundary (Fig. 2B). The windward portion of the Dinarides receives all of its moisture between September and May; in contrast, the leeward side receives a

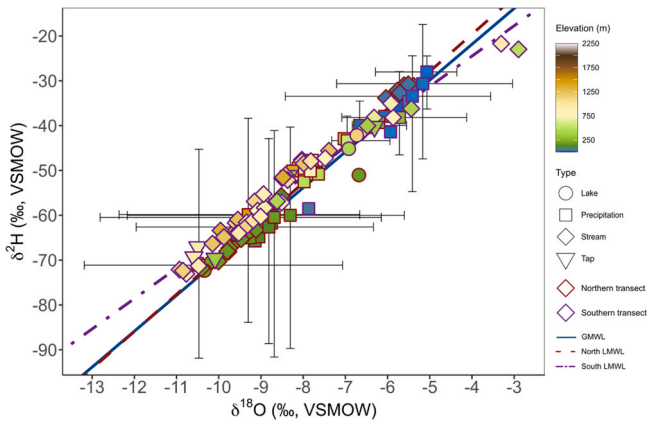

Fig. 7. Local meteoric water lines for our study area plotted alongside the global meteoric water line (GMWL, blue line). Northern local meteoric water line (red dashed line) falls above the GMWL at lower elevations; southern local meteoric water line (purple dash-dot line) falls above the GMWL at higher elevations. Points represent mean values of samples obtained from the various types of water including lake (circles), precipitation (squares), stream water (diamonds), and tap water (inverted triangles). Error bars represent the mean winter and summer values. Points are colored by mean basin elevation (m). Points highlighted in red are located in the northern part of the Dinarides, points highlighted in purple are located in the southern part of the Dinarides.

relatively large proportion of its annual precipitation (up to 50 ‰) in the summer (June, July, and August). This seasonality contrast is likely reflected in meteoric water d-excess values. Low d-excess values in summertime precipitation reflect generally higher relative humidity at the moisture source; in contrast, high d-excess values are characteristic of winter precipitation derived from low relative humidity at the moisture source (Pfahl and Sodemann, 2014; Xia et al., 2022). Thus, d-excess values in the Dinarides appear to trace the seasonal precipitation regimes across the Dinarides and the consequent variations in moisture sources across the range. We also note that our results are likely not influenced by temporal changes in stream water $\delta^{18}O$ and $\delta^{2}H$ values. Mountain stream waters across the globe typically exhibit low variability (often < 1 ‰) in $\delta^{18}O$ and $\delta^{2}H$ (Jasechko et al., 2016). Further, the three sites we visited in 2022 and 2025 (SW1, LW1, and BW4) show less than 0.5 ‰ differences in $\delta^{18}O$ and less than 3 ‰ differences in $\delta^{2}H$, with statistically identical d-excess values, suggesting that temporal variations in stream water isotope values are likely to be minimal and not likely to influence our conclusions.

Similar patterns are observed when examining only precipitation data (published in Hunjak et al., 2013). In precipitation, leeward stations have lower $\delta^{18}O$ values (approximately -9 ‰) compared to windward stations (approximately -6 ‰; Fig. 4). Similar trends in d-excess also appear when only examining the precipitation data; that is, high d-excess values in precipitation stations on the windward side of the Dinarides versus the leeward side. Again, this congruence in the spatial patterns of $\delta^{18}O$ and d-excess between our stream samples and precipitation samples suggests that the atmospheric processes that produce spatial patterns in $\delta^{18}O$ and d-excess are preserved in streams across the region. Low d-excess coastal samples from Hunjak et al. (2013) are likely lower than in other studies because they are averaging summer data that has high d-excess. We cannot correct for the difference in seasonal amount of precipitation because monthly data is not reported by Hunjak et al. (2013). We note that the precipitation $\delta^{18}O$ values may also be biased high due to the fact they are unweighted by precipitation amount, and there is higher $\delta^{18}O$ in the summer.

Interestingly, d-excess increases with elevation and peaks roughly at the location of the Dinarides crest at ca. 17 ‰ (see also Hunjak et al., 2013). Low d-excess values are found in low-elevation areas in the leeward side, which is consistent with summertime moisture. Meanwhile, the low elevation coastal samples have high and variable d-excess values consistent with predominantly wintertime Mediterranean moisture. This d-excess increase with elevation has been well-documented in other areas around the Mediterranean and in other orogens more generally (Liotta et al., 2006; Schemmel et al., 2013; Vreča et al., 2014; Masiol et al., 2021; Natali et al., 2022). For example, in the southern Apennines, high-elevation d-excess values have been observed as high as 45 ‰. The mechanism that generates high d-excess values at high elevation remains disputed, but one of the hypothesized mechanisms is the seeder-feeder mechanism, which posits that rain or snow that forms in response to orographic forcing evaporates during fall of the hydrometer. This enriches the surrounding vapor in ^{2}H relative to ^{18}O and this vapor is then recycled and uplifted to produce additional precipitation (Liotta et al., 2006; Masiol et al., 2021; Natali et al., 2022). Though analysis of the relevant mechanism that generates high d-excess at high elevation is beyond the scope of this paper, we note that the high d-excess values at high elevations in the Dinarides are somewhat muted relative to other orogens.

5.3. *Implications for paleoaltimetry and paleoenvironmental studies in the Dinarides*

The high $\delta^{18}O$ values at the coast and lower $\delta^{18}O$ values at the crest of the range are frequently observed in mountainous regions across the world and is known as the “altitude effect" (Rozanski et al., 1993; Poage and Chamberlain, 2001). This effect results from adiabatic uplift of moisture-laden air parcels; the resulting precipitation preferentially removes ^{18}O, resulting in lower $\delta^{18}O$ values at higher elevations. Beyond the crest of the range, meteoric water $\delta^{18}O$ values remain lower than at the coast but are slightly higher than meteoric water $\delta^{18}O$ values at the highest elevations of the Dinarides. These intermediate values in the lee of the range—in combination with our HYSPLIT and WAM modeling—suggest that meteoric waters reflect moisture with higher $\delta^{18}O$ values (i.e., Caves et al., 2015, Mix et al., 2019; Manser et al., 2024). In turn, this higher $\delta^{18}O$ moisture in the lee of the Dinarides reflects both an additional source (continental) as well as a shift in the seasonality of precipitation towards the summer, with attendant higher precipitation $\delta^{18}O$. A shift towards summertime moisture in the lee due to rising topography could be overwhelmed by a decrease in $\delta^{18}O$ due distillation over the Dinarides.

The clear decrease in $\delta^{18}O$ values with elevation and across the Dinarides suggests that authigenic minerals that form in the presence of meteoric water should preserve a signal of past topography. The extensive Miocene basins across the Dinarides (Mandic et al., 2009, 2011; Jiménez-Moreno et al., 2009; de Leeuw et al., 2010, 2011, 2012; Andrić et al., 2017; Sant et al., 2018; Andrić-Tomašević et al., 2021; Badurina et al., 2021; Brlek et al., 2021; Vranjković et al., 2024) may thus record past topography as encoded in the $\delta^{18}O$ values of authigenic minerals. Even basins located leeward of the Dinarides (e.g. Obradović et al., 1997; Andrić et al., 2015; Andrić-Tomašević et al., 2023) should reflect the past topography of the Dinarides, as these sites clearly receive a portion of their moisture from air parcels that have traversed the Dinarides.

However, many Miocene basins in the Dinarides are composed dominantly of lacustrine sediments; though there is little lake water $\delta^{18}O/\delta^{2}H$ data in the region, some of the lake $\delta^{18}O$ values compiled in this paper appears to be evaporatively enriched, as indicated by low d-excess values (Fig. 5) and a position far off the local meteoric water line (Fig. 7). This is also seen in lakes in Greece and North Macedonia (south of the Dinarides), where d-excess values range from -2 to -15 ‰ (Griffiths et al., 2002; Matzinger et al., 2006). Low d-excess values are also seen in high mountain regions such as the Himalayas and the Tibetan Plateau (Pande et al., 2000; Quade et al., 2011). While $\delta^{2}H$ cannot typically be measured in most types of authigenic minerals (though see Mix and Chamberlain, 2014), recent advances in analytical techniques have enabled measurements of ^{17}O, which is preserved in authigenic minerals such as clays and carbonates (Wostbrock et al., 2020; Wostbrock and Sharp, 2021; Aron et al., 2021; Ibarra et al., 2021; Kelson et al., 2023). Measurements of ^{17}O in authigenic minerals may permit quantitative constraints on the degree of evaporation, yielding estimates of the original meteoric water $\delta^{18}O$ value prior to experiencing evaporation (Passey and Ji, 2019).

With this in mind, the spatial pattern of d-excess across the Dinarides dominantly reflects the role of precipitation seasonality and its variation across the Dinarides. Given the greater sensitivity of ^{17}O to terrestrial hydroclimate processes and temperature (Xia et al., 2023), ^{17}O may be able to track how seasonality—particularly in leeward basins—has shifted in response to topographic growth of the Dinarides. Because precipitation $\delta^{18}O$ is strongly influenced by the season of precipitation, shifts in precipitation seasonality may obscure or amplify changes in $\delta^{18}O$ and therefore estimates of past topography. We note that the positive correlation of d-excess with elevation (Fig. 5) suggests that ^{17}O-excess may also vary with elevation (Xia et al., 2023). Thus, calculations of paleo-topography that utilize ^{17}O may need to account for variable ^{17}O-excess as elevation changes, particularly depending on the mechanism that elevates d-excess at high elevations. Ultimately, our analysis of d-excess patterns across the Dinarides indicates that measurements of ^{17}O in authigenic minerals may be useful in (1) discerning changes in precipitation seasonality in the past and (2) accounting for the effects of evaporation in the DLS on authigenic carbonates and the subsequent enrichment of ^{18}O in lacustrine carbonates.

6. Conclusions

We present new surface water samples across the Dinarides to constrain the modern-day pattern of meteoric water $\delta^{18}O$ and $\delta^{2}H$ across the Dinarides. Modern surface water $\delta^{18}O$ decreases with distance from coast and with increasing elevation. Surface water samples collected from the Adriatic coast have higher values of −6 ‰, while surface water samples collected from high-elevation basins have lower values of −11 ‰. The spatial distribution of $\delta^{18}O$ and d-excess across the Dinarides show two different sources of moisture. In combination with our HYSPLIT and WAM modeling, we interpret high d-excess values to show a strong influence of winter-time Mediterranean moisture on the windward side of the Dinarides. We interpret low d-excess in samples collected on the leeward side of the Dinarides to show a stronger influence of summertime moisture sourced from continental Europe. These same patterns are in agreement with published meteoric water $\delta^{18}O$ values and suggest that stream water $\delta^{18}O$ reflects precipitation $\delta^{18}O$.

Our study constrains the modern-day mechanisms that determine $\delta^{18}O$ patterns in the Dinarides and indicates that orographically forced rainout is the dominant effect that modifies precipitation and surface water $\delta^{18}O$ in the Dinarides region today. Nevertheless, changes in precipitation seasonality across the range, combined with shifting moisture sources, complicate the use of authigenic mineral $\delta^{18}O$ as a tracer of past topographic change. However, our analysis of controls on d-excess across the Dinarides suggests that ^{17}O-excess—a similar system to d-excess—may help resolve these other factors and permit a reconstruction of past topography. Thus, our findings have implications for work that seeks to understand the past topography of the Dinarides using authigenic and biogenic carbonate samples throughout the region.

CRediT authorship contribution statement

Jeremy K.C. Rugenstein: Writing – review & editing, Validation, Software, Resources, Project administration, Investigation, Funding acquisition, Conceptualization. **Maud J.M. Meijers:** Writing – review & editing, Validation, Supervision, Resources, Project administration, Investigation, Conceptualization. **Patrick W. Keys:** Writing – review & editing, Visualization, Software, Resources, Methodology. **Vedad Demir:** Resources. **Davor Pavelić:** Writing – review & editing, Supervision, Resources, Project administration, Investigation. **Oleg Mandic:** Writing – review & editing, Supervision, Resources, Project administration, Investigation, Conceptualization. **Nevena Andrić-Tomašević:** Writing – review & editing, Supervision, Resources, Project administration, Investigation, Conceptualization. **Marlene Löberbauer:** Writing – review & editing, Investigation. **Gabriela Sanchez Ortiz:** Writing – original draft, Visualization, Validation, Software, Investigation, Funding acquisition, Formal analysis, Data curation.

Declaration of Competing Interest

The authors declare the following financial interests/personal relationships which may be considered as potential competing interests. Gabriela Sanchez Ortiz reports financial support was provided by Geological Society of America. If there are other authors, they declare that they have no known competing financial interests or personal relationships that could have appeared to influence the work reported in this paper.

Acknowledgments

We thank Dan Reuss for help with laboratory measurements and Joel Leonard and Ana Maria Perez-Hincapie for help calculating basin-average elevation and hypsometry statistics. We also thank the members of the CSU GeoPAST group for feedback. This project was partially funded by a Geological Society of America Graduate Student Research Grant to Sanchez Ortiz. Rugenstein recieved funding from Colorado State University Warner College of Natural Resources. The authors acknowledge the financial support by the University of Graz for Open Access publishing

Appendix A. Supporting information

Supplementary data associated with this article can be found in the online version at doi:10.1016/j.ejrh.2026.103214.

Data availability

All new data is provided in Table 1. All compiled data is provided in the Supplementary data.

References

Andrić, N., Fügenschuch, B., Životić, D., Cvetković, V., 2015. The thermal history of the Miocene Ibar Basin (Southern Serbia): new constraints from apatite and zircon fission track and vitrinite reflectance data. Geol. Carpath. 66, 37–50. https://doi.org/10.1515/geoca-2015-0009.

Andrić, N., Sant, K., Matenco, L., Mandic, O., Tomljenović, B., Pavelić, D., Hrvatović, H., Demir, V., Ooms, J., 2017. The link between tectonics and sedimentation in asymmetric extensional basins: Inferences from the study of the Sarajevo-Zenica Basin. Mar. Petrol. Geol. 83, 305–332. https://doi.org/10.1016/j.marpetgeo.2017.02.024.

Andrić-Tomašević, N., Simić, V., Mandic, O., Životić, D., Suárez, M., García-Romero, E., 2021. An arid phase in the Internal Dinarides during the early to middle Miocene: inferences from Mg-clays in the Pranjani Basin (Serbia). Palaeogeogr. Palaeocl 562, 110–145. https://doi.org/10.1016/j.palaeo.2020.110145.

Andrić-Tomašević, N., Simić, V., Životić, D., Pavlović, A., Kluge, T., Beranoaguirre, A., Smit, J., Bechtel, A., 2023. Tectonically induced travertine deposition in the Levač intramountain basin (Central Serbia). Sedimentology 71, 1214–1244. https://doi.org/10.1111/sed.13171.

Aron, P.G., Levin, N.E., Beverly, E.J., Huth, T.E., Passey, B.H., Pelletier, E.M., Poulsen, C.J., Winkelstern, I.Z., Yarian, D.A., 2021. Triple oxygen isotopes in the water cycle. Chem. Geol. 565, 120026. https://doi.org/10.1016/j.chemgeo.2020.120026.

Badurina, L., Šegvić, B., Mandic, O., Slovenec, D., 2021. Miocene tuffs from the Dinarides and Eastern Alps as proxies of the Pannonian Basin lithosphere dynamics and tropospheric circulation patterns in Central Europe. J. Geol. Soc. Lond. 178. https://doi.org/10.1144/jgs2020-262.

Baldwin, J., Vecchi, G., 2016. Influence of the Tian Shan on Arid Extratropical Asia. J. Clim. 29, 5741–5762. https://doi.org/10.1175/JCLI-D-15-0490.1.

Bennett, R., Hreinsdóttir, S., Buble, G., Bašić, T., Bačić, Z., Marjanović, M., Casale, G., Gendaszek, A., Cowan, D., 2018. Eocene to present subduction of southern Adria mantle lithosphere beneath the Dinarides. Geology 36, 3–6. https://doi.org/10.1130/G24136A.1.

Blisniuk, P.M., Stern, L.A., 2005. Stable isotope paleoaltimetry: A critical review. Am. J. Sci. 305, 1033–1074.

Brlek, M., Gaynor, S.P., Mongelli, G., Bauluz, B., Sinisi, R., Brčić, V., Peytcheva, I., Mišur, I., Tapster, S., Trinajstić, N., Laitla, E., Yuste, A., Šuica, S., Grizelj, A., Kukoč, D., Schaltegger, U., 2021. Karst bauxite formation during Miocene Climate Optimum (central Dalmatia, Croatia): mineralogical, compositional and geochronological perspectives. Int. J. Earth Sci. 110, 2899–2922. https://doi.org/10.1007/s00531-021-002091-z.

Burić, M. (2010). Atlas voda Crne Gore. Crnogorska akademija nauka i umjetnosti.

Caves, J.K., Winnick, M.J., Graham, S.A., Sjostrom, D.J., Mulch, A., Chamberlain, C.P., 2015. Role of the westerlies in Central Asia climate over the Cenozoic. Earth Planet. Sci. Lett. 428, 33–43. https://doi.org/10.1016/j.epsl.2015.07.23.

Caves, J.K., Baysdashov, B.U., Zhamangara, A., Ritch, A.J., Ibarra, D.E., Sjostrom, D.J., Mix, H.T., Winnick, M.J., Chamberlain, C.P., 2017. Late Miocene uplift of the Tian Shan and Altai and reorganization of Central Asia climate. GSA Today 27, 19–26. https://doi.org/10.1130/GSATG305A.1.

Chamberlain, C.P., Poage, M.A., 2000. Reconstructing the paleotopography of mountain belts from the isotopic composition of authigenic minerals. Geology 28, 115–118. https://doi.org/10.1130/0091-7613(2000)28<115:RTPOMB>2.0.CO;2.

Dansgaard, W., 1964. Stable isotopes in precipitation. Tellus 16, 436–468. https://doi.org/10.3402/tellusa.v16i48993.

Dee, D.P., Uppala, S.M., Simmons, A.J., Berrisford, P., Poli, P., Kobayashi, S., Andrae, U., Balmaseda, M.A., Balsamo, G., Bauer, P., Bechtold, P., Berljaars, A.C., Van De Berg, L., Bidlot, J., Bormann, N., Delsol, C., Dragani, R., Fuentes, M., Geer, A.J., Haimberger, L., Healey, S.B., Hersbach, H., Hólm, E.V., Isaksen, L., Kållberg, P., Köhler, M., Matricardi, M., Mcnally, A.P., Monge-Sanz, B.M., Morcrette, J.-J., Park, B.-K., Peubey, C., De Rosnay, P., Tavolato, C., Thèpaut, J.-N., Vitart, F., 2011. The ERA-Interim reanalysis: configuration and performance of the data assimilation system. Q. J. Roy. Meteor. Soc. 137, 553–597. https://doi.org/10.1002/qj.828.

Draxler, R.R., Hess, G.D., 1998. An overview of the HYSPLIT_4 modelling system for trajectories, dispersion and deposition. Aust. Meteorol. Mag. 47, 295–308.

Driscoll, E., Needham, M.R., Keys, P.W., Rugenstein, J.K.C., 2024. Cenozoic stable isotope constraints on the Eurasian continental interior hydroclimate response to high CO_2. Earth Planet. Sci. Lett. 630, 118623. https://doi.org/10.1016/j.epsl.2024.118623.

Forest, C.E., Molnar, P., Emanuel, K.A., 1995. Palaeoaltimetry from energy conservation principles. Nature 374, 347–350.

Forte, A.M., Whipple, K.X., 2019. Short Communication: The Topographic Analysis Kit (TAK) for TopoToolbox. Earth Surf. Dynam 7, 87–95. https://doi.org/10.5194/esurf-7-87-2019.

Gat, J.R. (2010): Isotope Hydrology: A Study of the Water Cycle. World Scientific 6.

Gat, J.R., Carmi, I., 1970. Evolution of the isotopic composition of atmospheric waters in the Mediterranean Sea area. J. Geophys. Res. 75, 3039–3048. https://doi.org/10.1029/jc075i015p03039.

Gat, J.R., Dansgaard, W., 1972. Stable isotopes of the fresh water occurences in Israel and the Northern Jordan Rift Valley. J. Hydrol. 16, 177–212. https://doi.org/10.1016/0022-1694(72)90052-2.

Gat, J.R., Klein, B., Kushnir, Y., Roether, W., Wernli, H., Yam, R., Shemesh, A., 2003. Isotope composition of air moisture over the Mediterranean Sea: an index of the air-sea interaction pattern. Tellus B 55 (5), 953–965. https://doi.org/10.3402/tellusb.v55i5.16395.

Griffiths, H.I., Reed, J.M., Leng, M.J., Ryan, S., Petkovski, S., 2002. The recent palaeoecology and conservation status of Balkan Lake Dojran. Biol. Conserv 104, 35–49. https://doi.org/10.1016/S0006-3207(01)00152-5.

Handy, M.R., Giese, J., Schmid, S.M., Pleuger, J., Spakman, W., Onuzi, K., Ustaszewski, K., 2019. Coupled crust-mantle response to slab tearing, bending, and rollback along the Dinaride-Hellenide Orogen. Tectonics 38, 2803–2828. https://doi.org/10.1029/2019TC005524.

Harzhauser, M., Mandic, O., 2008. Neogene lake systems of Central and South-Eastern Europe: Faunal diversity, gradients and interrelations. Palaeogeogr. Palaeocl. 260, 417–434. https://doi.org/10.1016/j.palaeo.2007.12.013.

Harzhauser, M., Mandic, O., Latal, C., Kern, A., 2012. Stable isotope composition of the Miocene Dinaride Lake System deduced from its endemic mollusk fauna. Hydrobiologia 682, 27–46. https://doi.org/10.1007/s10750-011-0618-3.

Hoke, G.D., Liu-Zeng, J., Hren, M.T., Wissink, G.K., Garzione, C.N., 2014. Stable isotopes reveal high southeast Tibetan Plateau margin since the Paleogene. Earth Planet. Sci. Lett. 394, 270–278. https://doi.org/10.1016/j.epsl.2014.03.007.

Hunjak, T., Lutz, H.O., Roller-Lutz, Z., 2013. Stable isotope composition of the meteoric precipitation in Croatia. Isot. Environ. Heal. S. 49, 336–345. https://doi.org/10.1080/10256016.2013.816697.

Ibarra, D.E., Kukla, T., Methner, K.A., Mulch, A., Chamberlain, C.P., 2021. Reconstructing past elevations from triple oxygen isotopes of lacustrine chert: Application to the Eocene Nevadaplano, Elko Basin, Nevada, United States. Front. Earth Sci. 9, 628868. https://doi.org/10.3389/feart.2021.628868.

Jasechko, S., Kirchner, J.W., Welker, J.M., McDonnell, J.J., 2016. Substantial proportion of global streamflow less than three months old. Nat. Geosci. 9. https://doi.org/10.1038/NGEO2636.

Jiménez-Moreno, G., De Leeuw, A., Mandic, O., Harzhauser, M., Pavelić, D., Krijgsman, W., Vranjković, A., 2009. Integrated stratigraphy of the Early Miocene lacustrine deposits of Pag Island (SW Croatia): Palaeovegetation and environmental changes in the Dinaride Lake System. Palaeogeogr. Palaeocl 280, 193–206. https://doi.org/10.1016/j.palaeo.2009.05.018.

Kelson, J.R., Huth, T.E., Passey, B.H., Levin, N.E., Petersen, S.V., Ballato, P., Beverly, E.J., Breecker, D.O., Hoke, G.D., Hudson, A.M., Ji, H., Licht, A., Oerter, E.J., Quade, J., 2023. Triple oxygen isotope compositions of globally distributed soil carbonates record widespread evaporation of soil waters. Geochim. Cosmochim. Acta 355, 138–160. https://doi.org/10.1016/j.gca.2023.06.034.

Keys, P.W., Wang-Erlandsson, L., 2018. On the social dynamics of moisture recycling. Earth Syst. Dynam 9, 829–847. https://doi.org/10.5194/esd-9-829-2018.

Keys, P.W., Van der Ent, R.J., Gordon, L.J., Hoff, H., Nikoli, R., Savenije, H.H.G., 2012. Analyzing precipitationsheds to understand the vulnerability of rainfall dependent regions. Biogeosciences 9, 733–746. https://doi.org/10.5194/bg-9-733-2012.

Keys, P.W., Wang-Erlandsson, L., Gordon, L.J., 2018. Megacity precipitationsheds reveal tele-connected water security challenges. Public Libr. Sci. ONE 13, e0194311. https://doi.org/10.1371/journal.pone.0194311.
Krstić, N., Savić, L., Jovanović, G., Bodor, E., 2003. Lower Miocene lakes of the Balkan Land. Acta Geol. Hung. 46, 291–299. https://doi.org/10.1556/ageol.46.2003.3.4.
Krstić, N., Savić, L., Jovanović, G., 2012. The Neogene Lakes of the Balkan Land. Geol. Anal. Balk. poluostrva (73), 37–60. https://doi.org/10.2298/GABP1273037K.
Kukla, T., Rugenstein, J.K.C., Ibarra, D.E., Winnick, M.J., Strömberg, C.A.E., Chamberlain, C.P., 2022. Drier winters drove Cenozoic open habitat expansion in North America. e2021AV000566 AGU Adv. 3. https://doi.org/10.1029/2021AV000566.
Lechler, A.R., Galewsky, J., 2013. Refining paleoaltimetry reconstructions of the Sierra Nevada, California, using air parcel trajectories. Geology 41, 259–262. https://doi.org/10.1130/G33553.1.
Lee, J.-E., Risi, C., Fung, I., Worden, J., Scheepmaker, R.A., Lintner, B., Frankenberg, C., 2012. Asian monsoon hydrometeorology from TES and SCIAMACHY water vapor isotope measurements and LMDZ simulations: Implications for speleothem climate record interpretation. J. Geophys. Res. 117, D15112. https://doi.org/10.1029/2011JD017133.
de Leeuw, A., Mandic, O., Vranjković, A., Pavelić, D., Harzhauser, M., Krijgsman, W., Kuiper, K., 2010. Chronology and integrated stratigraphy of the Miocene Sinj Basin (Dinaride Lake System, Croatia). Palaeogeogr. Palaeocl 292, 155–167. https://doi.org/10.1016/j/palaeo.2010.03.040.
de Leeuw, A., Mandic, O., Krijgsman, W., Kuiper, K., Hrvatović, H., 2011. A chronostratigraphy for the Dinaride Lake System deposits of the Livno-Tomislavgrad Basin: the rise and fall of a long-lived lacustrine environment. Stratigraphy 8, 29–43.
de Leeuw, A., Mandic, O., Krijgsman, W., Kuiper, K., Hrvatović, H., 2012. Paleomagnetic and geochronologic constraints on the geodynamic evolution of the Central Dinarides. Tectonophysics 530-531, 286–298. https://doi.org/10.1016/j.tecto.2012.01.004.
Leng, M.J., Marshall, J.D., 2004. Palaeoclimate interpretation of stable isotope data from lake sediment archives. Quat. Sci. Rev. 23, 811–831. https://doi.org/10.1016/j.quascirev.2003.06.012.
Liotta, M., Favara, R., Valenza, M., 2006. Isotopic composition of the precipitations in the central Mediterranean: Origin marks and orographic precipitation effects. J. Geophys. Res. 111, D19302. https://doi.org/10.1029/2005JD006818.
Mandic, O., Pavelić, D., Harzhauser, M., Zupanič, J., Reischenbacher, D., Sachsenhofer, R.F., Tadej, N., Vranjković, A., 2009. Depositional history of the Miocene Lake Sinj (Dinaride Lake System, Croatia): a long-lived hard-water lake in a pull-apart tectonic setting. J. Paleolimnol. 41, 431–452. https://doi.org/10.1007/s10933-008-9235-1.
Mandic, O., De Leeuw, A., Vukovic, B., Krijgsman, W., Harzhauser, M., Kuiper, K.F., 2011. Palaeoenvironmental evolution of Lake Gacko (NE Bosnia and Herzegovina): impact of the Middle Miocene Climatic Optimum on the Dinaride Lake System. Palaeogeogr. Palaeocl 299 (3-4), 475–492. https://doi.org/10.1016/j.palaeo.2010.11.024.
Mandic, O., Harzhauser, M., Neubauer, T.A., 2020. Taxonomy, palaeoecology and stratigraphy of the middle Miocene mollusk fauna from the Gračanica coal pit near Bugojno in Bosnia and Herzegovina. Palaeobio. Palaeoenv 100, 519–549. https://doi.org/10.1007/s12549-020-00423-6.
Manser, L., Kukla, T., Rugenstein, J.K.C., 2024. Stable isotope evidence for long-term stability of large-scale hydroclimate in the Neogene North American Great Plains. Clim 20 (4). https://doi.org/10.5194/egusphere-2023-2075.
Marković, T., Karlović, I., Perčec Tadić, M., Larva, O., 2020. Application of stable water isotopes to improve conceptual model of alluvial aquifer in the Varaždin area. Water 12, 379. https://doi.org/10.3390/w12020379.
Masiol, M., Zannoni, D., Stenni, B., Dreossi, G., Zini, L., Calligaris, C., Karlicek, D., Michelini, M., Flora, O., Cucchi, F., Treu, F., 2021. Spatial distribution and interannual trends of d18O, d2H, and deuterium excess in precipitation across North-Eastern Italy. J. Hydrol. 598, 125749. https://doi.org/10.1016/j.jhydrol.2020.125749.
Matzinger, A., Jordanoski, M., Veljanoska-Sarafiloska, E., Sturm, M., Müller, B., Wüest, A., 2006. Is Lake Prespa jeopardizing the ecosystem of ancient Lake Ohrid? Hydrobiologia 553, 89–109. https://doi.org/10.1007/s10750-005-6427-9.
Mix, H.T., Chamberlain, C.P., 2014. Stable isotope records of hydrologic change and paleotemperature from smectite in Cenozoic western North America. Geochim. Cosmochim. Acta 141, 532–546. https://doi.org/10.1016/j.gca.2014.07.008.
Mix, H.T., Mulch, A., Kent-Corson, M.L., Chamberlain, C.P., 2011. Cenozoic migration of topography in the North American Cordillera. Geology 39, 87–90. https://doi.org/10.1130/G31450.1.
Mix, H.T., Rugenstein, J.K.C., Reilly, S.P., Ritch, A.J., Winnick, M.J., Kukla, T., Chamberlain, C.P., 2019. Atmospheric flow deflection in the late Cenozoic Sierra Nevada. Earth Planet. Sci. Lett. 518, 76–85. https://doi.org/10.1016/j.epsl.2019.04.050.
Molnar, P., England, P., 1990. Late Cenozoic uplift of mountain ranges and global climate change: chicken or egg? Nature 346, 29–34. https://doi.org/10.1038/346029a0.
Natali, S., Doveri, M., Giannecchini, R., Baneschi, I., Zanchetta, G., 2022. Is the deuterium excess in precipitation a reliable tracer of moisture sources and water resources fate in the western Mediterranean? New insights from Apuan Alps (Italy). J. Hydrol. 614, 128497. https://doi.org/10.1016/j.jhydrol.2022.128497.
Neubauer, T.A., Harzhauser, M., Georgopoulou, E., Kroh, A., Mandic, O., 2015c. Tectonics, climate, and the rise and demise of continental aquatic species richness hotspots. Proc. Natl. Acad. Sci. 112, 11478–11483. https://doi.org/10.1073/pnas.1503992112.
Neubauer, T.A., Harzhauser, M., Kroh, A., Georgopoulou, E., Mandic, O., 2015a. A gastropod-based biogeographic scheme for the European Neogene freshwater systems. EarthSci. Rev. 143, 98–116. https://doi.org/10.1016/j.earscirev.2015.01.010.
Neubauer, T.A., Mandic, O., Harzhauser, M., 2015b. The freshwater mollusc fauna of the Middle Miocene Lake Drniš (Dinaride Lake System, Croatia): a taxonomic and systematic revision. Austrian J. Earth Sci. 108, 15–67. https://doi.org/10.17738/ajes.2015.0013.
Neubauer, T.A., Mandic, O., Jovanović, G., Harzhauser, M., 2020. The Serbian Lake System: a stepping stone for freshwater molluscs in the middle Miocene. Pap. Palaeontol. 6, 533–569. https://doi.org/10.1594/PANGAEA.909449.
Obradović, J., Djurdjević-Colson, J., Vasić, N., 1997. Phytogenic lacustrine sedimentation - oil shales in Neogene from Serbia, Yugoslavia. J. Paleolimnol. 18, 351–364. https://doi.org/10.1023/A:1007907109399.
Oster, J.L., Montañez, I.P., Kelley, N.P., 2012. Response of a modern cave system to large seasonal precipitation variability. Geochim. Cosmochim. Acta 91, 92–108. https://doi.org/10.1016/j.gca.2012.05.027.
Pamić, J., 2002. The Sava-Vardar Zone of the Dinarides and Hellenides versus the Vardar Ocean. Eclogae Geol. Helv. 95, 99–113. https://doi.org/10.5169/seals-168948.
Pande, K., Padia, J.T., Ramesh, R., Sharma, K.K., 2000. Stable isotope systematics of surface water bodies in the Himalayan and Trans-Himalayan (Kashmir) region. J. Earth Syst. Sci. 109, 109–115. https://doi.org/10.1007/BF02719154.
Passey, B.H., Ji, H., 2019. Triple oxygen isotope signatures of evaporation in lake waters and carbonates: A case study from the western United States. Earth Planet. Sci. Lett. 518, 1–12. https://doi.org/10.1016/j.epsl.2019.04.026.
Pavelić, D., Kovačić, M., Banak, A., Jiménez-Moreno, G., Marković, F., Premužak, L., Tibljaš, D., Belak, M., 2016. Early Miocene European loess: A new record of aridity in southern Europe. GSA Bull. 128, 110–121. https://doi.org/10.1130/B31280.1.
Pavelić, D., Kovačić, M., Tibljaš, D., Galić, I., Marković, F., Pavičić, I., 2022. The closed transition from a closed to an open lake in the Pannonian Basin System (Croatia) during the Miocene Climatic Optimum: Sedimentological evidence of Early Miocene regional aridity. Palaeogeogr. Palaeocl 586, 110786. https://doi.org/10.1016/j.palaeo.2021.110786.
Pfahl, S., Sodemann, H., 2014. What controls deuterium excess in global precipitation? Clim 10, 771–781. https://doi.org/10.5194/cp-10-771-2014.
Poage, M.A., Chamberlain, C.P., 2001. Empirical relationships between elevation and the stable isotope composition of precipitation and surface waters: Considerations for studies of paleoelevation change. Am. J. Sci. 301, 1–15. https://doi.org/10.2475/ajs.301.1.1.
Putman, A.L., Fiorella, R.P., Bowen, G.J., Cai, Z., 2019. A global perspective on local meteoric water lines: meta-analytic insight into fundamental controls and practical constraints. Water Resour. Res. 55, 6896–6910. https://doi.org/10.1029/2019WR025181.
Quade, J., Breecker, D.O., Daëron, M., Eiler, J., 2011. The Paleoaltimetry of Tibet: An Isotopic Perspective. Am. J. Sci. 311, 77–115. https://doi.org/10.2475/02.2011.01.

Rowley, D.B., Garzione, C.N., 2007. Stable isotope-based paleoaltimetry. Annu. Rev. Earth Pl. Sc. 35, 463–508. https://doi.org/10.1146/annurev.earth.35.031306.140155.
Rowley, D.B., Pierrehumbert, R.T., Currie, B.S., 2001. A new approach to stable isotope-based paleoaltimetry: implications for paleoaltimetry and paleohypsometry of the High Himalaya since the Late Miocene. Earth Planet. Sci. Lett. 188, 253–268. https://doi.org/10.1016/S0012-821X(01)00324-7.
Rozanski, K., Araguás-Araguás, L., Gonfiantini, R., 1993. Isotopic patterns in modern global precipitation. Clim. Change Cont. Isot. Rec. 78, 1–36.
Rugenstein, J.K.C., Methner, K., Kukla, T., Mulch, A., Lüdecke, T., Fiebig, J., Wegmann, K.W., Zeitler, P.K., Chamberlain, C.P., 2022. Clumped isotope constraints on warming and precipitation seasonality in Mongolia following Altai uplift. Am. J. Sci. 322, 28–54. https://doi.org/10.2475/01.2022.02.
San Jose, M., Rugenstein, J.K.C., Cosentino, D., Faccenna, C., Fellin, M.G., Ghinassi, M., Martini, I., 2020. Stable isotope evidence for rapid uplift of the central Apennines since the late Pliocene. Earth Planet. Sci. Lett. 544, 116376. https://doi.org/10.1016/j.epsl.2020.1163769.
Sant, K., Andrić, N., Mandic, O., Demir, V., Pavelić, D., Rundić, L., Hrvatović, H., Matenco, L., Krijgsman, W., 2018. Magneto-biostratigraphy and paleoenvironments of the Miocene freshwater sediments of the Sarajevo-Zenica Basin. Palaeogeogr. Palaeocl 506, 48–69. https://doi.org/10.1016/j.palaeo.2018.06.009.
Schemmel, F., Mikes, T., Rojay, B., Mulch, A., 2013. The impact of topography on isotopes in precipitation across the Central Anatolian Plateau (Turkey). Am. J. Sci. 313, 61–80. https://doi.org/10.2475/02.2013.01.
Schiemann, R., Lüthi, D., Schär, C., 2009. Seasonality and interannual variability of the westerly jet in the Tibetan Plateau region. J. Clim. 22, 2940–2957. https://doi.org/10.1175/2008JCLI2625.1.
Schmid, S., Bernoulli, D., Fügenschuh, B., Matenco, L., Schefer, S., Schuster, R., Tischler, M., Ustaszewski, K., 2008. The Alpine-Carpathian-Dinaric orogenic system: correlation and evolution of tectonic units. Swiss J. Geosci. 101, 139–183. https://doi.org/10.1007/s00015-008-1247-3.
Schwanghart, W., Scherler, D., 2014. Short Communication: TopoToolbox 2 – MATLAB-based software for topographic analysis and modeling in Earth surface sciences. Earth Surf. Dynam 2, 1–7. https://doi.org/10.5194/esurf-2-1-2014.
Sharp, Z. (2017): Principles of Stable Isotope Geochemistry, 2nd Edition. doi: 10.25844/h9q1-0p82.
Sjostrom, D.J., Welker, J.M., 2009. The influence of air mass source on the seasonal isotopic composition of precipitation, eastern USA. J. Geochem. Explor 102, 103–112. https://doi.org/10.1016/j.gexplo.2009.03.001.
Spaur, S., Koning, D.J., Heizler, M., Aby, S., Williamson, G., Knott, J.R., Acost, R.P., Rugenstein, J.K.C., 2025. The Hydroclimate and Environmental Response to Middle Miocene Warming in the Southwestern USA: Stable Isotope Evidence. e2024PA005056 Paleoceanogr. Paleoclimatology 40. https://doi.org/10.1029/2024PA005056.
Stein, A.F., Draxler, R.R., Rolph, G.D., Stunder, B.J.B., Cohen, M.D., Ngan, F., 2015. NOAA's HYSPLIT atmospheric transport and dispersion modeling system. Bull. Am. Meteorol. Soc. 96, 2059–2077. https://doi.org/10.1175/BAMS-D-14-00110.1.
Šumanovac, F., Markušić, S., Engelsfeld, T., Jurković, K., Orešković, J., 2017. Shallow and deep lithosphere slabs beneath the Dinarides from teleseismic topography as the result of the Adriatic lithosphere downwelling. Tectonophysics 712-713, 523–541. https://doi.org/10.1016/j.tecto.2017.06.018.
van der Ent, R.J., Savenije, H.H.G., 2013. Oceanic sources of continental precipitation and the correlation with sea surface temperature. Water Resour. Res. 49, 3993–4004. https://doi.org/10.1002/wrcr.20296.
van der Ent, R.J., Savenije, H.H.G., Schaefli, B., Steele-Dune, S.C., 2010. Origin and fate of atmospheric moisture over continents. Water Resour. Res. 46, W09525. https://doi.org/10.1029/2010WR009127.
Vranjković, A., Gierlowski-Kordesch, E., Mandic, O., Aljnović, D., Dragičević, I., Harzhauser, M., Kuiper, K., Brčić, V., Pavelić, D., 2024. Sedimentology and paleoenvironmental analysis of a karstic shallow carbonate lake (Early-Middle Miocene, Sinj Basin, Croatia). Depos. Rec. 11, 121–146. https://doi.org/10.1002/dep2.292.
Vreča, P., Krajcar Bronić, I., Horvatinčić, N., Barešić, J., 2006. Isotopic characteristics of precipitation in Slovenia and Croatia: Comparisons of continental and maritime stations. J. Hydrol. 330, 457–469. https://doi.org/10.1016/j.jhydrol.2006.04.005.
Vreča, P., Krajcar Bronić, I., Leis, A., Demšar, M., 2014. Isotopic composition of precipitation at the station Ljubljana (Reaktor), Slovenia - period 2007-2010. Geologija 52, 217–230. https://doi.org/10.5474/geologija.2014.019.
Willet, S.D., 1999. Orogeny and orography: The effects of erosion on the structure of mountain belts, 28,957-28,981 J. Geophys. Res. Sol. Ea 104. https://doi.org/10.1029/1999JB900248.
Wostbrock, J.A.G., Sharp, Z.D., 2021. Triple oxygen isotopes in silica-water and carbonate-water systems. Rev. Miner. Geochem 86, 367–400. https://doi.org/10.2138/rmg.2021.86.11.
Wostbrock, J.A.G., Brand, U., Coplen, T.B., Swart, P.K., Carlson, S.J., Brearley, A.J., Sharp, Z.D., 2020. Calibration of carbonate-water triple oxygen isotope fractionation: seeing through diagenesis in ancient carbonates. Geochim. Cosmochim. Acta 288, 360–388. https://doi.org/10.1016/j.gca.2020.07.045.
Xia, Z., Welker, J.M., Winnick, M.J., 2022. The seasonality of deuterium excess in non-polar precipitation. e2021GB007245 Glob. Biogeochem. Cy. 36. https://doi.org/10.1029/2021GB007245.
Xia, Z., Surma, J., Winnick, M.J., 2023. The response and sensitivity of deuterium and ^{17}O excess parameters in precipitation to hydroclimate processes. EarthSci. Rev. 242, 104432. https://doi.org/10.1016/j.earscirev.2023.104432.
Zaninović, K., Gajić-Čapka, M., Perčec Tadić, M., Vučetić, M., Milković, J., Bajić, A., Cindrić, K., Cvitan, L., Katušin, Z., Kaučić, D., Likso, T., Lončar, E., Lončar, Z., Mihajlović, D., Pandžić, K., Patarčić, M., Srnec, L., Vučetić, V., 2008. Klimatski atlas Hrvatske/Climate atlas of Croatia, 1961-1990. Meteorological and Hydrological Service of Croatia, pp. 1971–2000.
Zhu, L., Fan, M., Hough, B., Li, L., 2018. Spatiotemporal distribution of river water stable isotope compositions and variability of lapse rate in the central Rocky Mountains: Controlling factors and implications for paleoelevation reconstruction. Earth Planet. Sci. Lett. 496, 215–226. https://doi.org/10.1016/j.epsl.2018.05.047.